Chinese Journal of Natural Medicines

Atractylodis Rhizoma–Atractylodis Macrocephala Rhizoma herbal pair restores intestinal mucosal barrier function in ulcerative colitis *via* activating Epac1/Rap1 pathway and inhibiting PI3K/AKT pathway

Xuecheng Yu, Wenlong Su, Peng Huang, Zengxiang Gao, Yunya Lin, Jiyuan Tu, Yan Cao, Yanju Liu, Linlin Chen, Guosheng Cao

Citation: Xuecheng Yu, Wenlong Su, Peng Huang, Zengxiang Gao, Yunya Lin, Jiyuan Tu, Yan Cao, Yanju Liu, Linlin Chen, Guosheng Cao, Atractylodis Rhizoma–Atractylodis Macrocephala Rhizoma herbal pair restores intestinal mucosal barrier function in ulcerative colitis *via* activating Epac1/Rap1 pathway and inhibiting PI3K/AKT pathway, Chinese Journal of Natural Medicines, 2026, 24(3), 313–325. doi: 10.1016/S1875–5364(26)61106–5.

View online: https://doi.org/10.1016/S1875–5364(26)61106–5

Chinese Journal of Natural Medicines 24 (2026) 313-325

Contents lists available at ScienceDirect

Chinese Journal of Natural Medicines

journal homepage: www.cjnmcpu.com/

Original article

Atractylodis Rhizoma-Atractylodis Macrocephala Rhizoma herbal pair restores intestinal mucosal barrier function in ulcerative colitis *via* activating Epac1/Rap1 pathway and inhibiting PI3K/AKT pathway

Xuecheng Yu[a,Δ], Wenlong Su[a,Δ], Peng Huang[a,Δ], Zengxiang Gao[a], Yunya Lin[b], Jiyuan Tu[a,b], Yan Cao[a,b], Yanju Liu[a,b], Linlin Chen[b,c,*], Guosheng Cao[a,b,*]

[a] *College of Pharmacy, Hubei University of Chinese Medicine, Wuhan 430065, China*
[b] *Hubei Shizhen Laboratory, Wuhan 430065, China*
[c] *Key Laboratory of Traditional Chinese Medicine Resource and Compound Prescription, Ministry of Education, Hubei University of Chinese Medicine, Wuhan 430065, China*

ARTICLE INFO

Article history:
Received 4 February 2025
Revised 27 April 2025
Accepted 8 May 2025
Available online 20 March 2026

Keywords:
Ulcerative colitis
Atractylodis Rhizoma-Atractylodis Macrocephala Rhizoma
Epac1/Rap1
PI3K/AKT
Intestinal barrier

ABSTRACT

Ulcerative colitis (UC) is a persistent, diffuse intestinal inflammation and ranks among the most challenging chronic diseases worldwide. *Atractylodes lancea* (Thunb.) DC. and *Atractylodis macrocephala* Koidz. are traditional Chinese medicines (TCMs) with a long history of clinical application, particularly for gastrointestinal disorders. Both Atractylodis Rhizoma (AR) and Atractylodis Macrocephala Rhizoma (AM) have shown significant efficacy in managing UC; however, the underlying mechanism by which the AR-AM herbal pair promotes intestinal mucosal healing remains poorly understood. The therapeutic effects of the ethanolic extract of AR-AM (EEAR-AM) were evaluated in a murine UC model induced by dextran sodium sulfate (DSS). A network pharmacology approach was employed to explore the anti-UC properties of EEAR-AM, including identification of active compounds, prediction of potential targets, and construction of a protein-protein interaction (PPI) network. Gene Ontology (GO) and Kyoto Encyclopedia of Genes and Genomes (KEGG) analyses were subsequently performed to preliminarily elucidate the mechanisms of EEAR-AM in UC treatment. Finally, the proposed molecular mechanisms were validated in both DSS-induced UC mice and Caco-2 cells. *In vivo* results demonstrated that EEAR-AM significantly attenuated DSS-induced weight loss, reduced colon shortening, lowered the disease activity index (DAI) score, and modulated the spleen coefficient. Moreover, EEAR-AM improved colonic tissue architecture, reduced inflammatory infiltration, restored goblet cell density, enhanced mucin MUC2 expression, and elevated levels of tight junction (TJ) proteins. Additionally, EEAR-AM suppressed the expression of matrix metalloproteinase 2 (MMP-2) and MMP-9. Network pharmacology analyses indicated that EEAR-AM may ameliorate intestinal mucosal dysfunction through modulation of the exchange protein directly activated by cAMP 1 (Epac1)/Ras-associated protein 1 (Rap1) pathway and phosphatidylinositol 3-kinase (PI3K)/protein kinase B (AKT) pathways. These actions potentially enhance cellular barrier integrity and reduce the release of inflammatory mediators. Western blotting results confirmed that EEAR-AM activated the Epac1/Rap1 pathway while downregulating the PI3K/AKT pathway in both DSS-induced UC mice and Caco-2 cells, consistent with predictions from network pharmacology. This study represents the first evidence that the EEAR-AM herbal pair improves intestinal mucosal barrier function in UC, with therapeutic effects likely mediated by activation of the Epac1/Rap1 pathway and inhibition of the PI3K/AKT pathway.

1. Introduction

Ulcerative colitis (UC) is a chronic, relapsing inflammatory bowel disease that primarily involves the mucosa of the colon and rectum. Common clinical manifestations include diarrhea, abdominal pain, and hematochezia. The condition typically progresses insidiously and poses substantial therapeutic challenges, significantly increasing the risk of colorectal cancer development [1, 2]. The rising global prevalence of UC highlights an urgent need for improved treatment strategies. Although conventional therapies, such as corticosteroids and aminosalicylates, can alleviate symptoms, they are often associated with high costs and notable adverse effects. This underscores the necessity of identifying therapeutic options that are effective, cost-efficient, and minimally toxic [3].

The exact etiology and pathophysiological mechanisms of UC remain incompletely understood. Evidence suggests that multiple interacting factors contribute to both the onset and progression of the disease, including genetic susceptibility, environment-

* Corresponding author.
E-mail addresses: lin-lin.chen@hotmail.com (L. Chen); caoguosheng2006@163.com (G. Cao)
Δ These authors contributed equally to this work.

https://doi.org/10.1016/S1875-5364(26)61106-5

al triggers, dysregulated immune responses, and impairment of the intestinal barrier. Notably, the intestinal mucosal barrier plays a pivotal role in maintaining gastrointestinal homeostasis and is closely implicated in UC pathogenesis [4]. Upon exposure to external stressors, the integrity of this barrier is compromised, leading to increased epithelial permeability. This disruption facilitates microbial dysbiosis and enables translocation of pathogens and their metabolites across the epithelium, potentially triggering or amplifying local inflammation. Persistent damage may culminate in mucosal ulceration; thus, restoration of the intestinal mucosal barrier is essential for improving gut function and mitigating UC-related clinical symptoms [5].

Traditional Chinese medicine (TCM) has emerged as a promising approach for UC management, attributed to its multi-target effects and favorable safety profile, suggesting potential for promoting mucosal repair [6]. A core principle of TCM is herb compatibility, which underpins synergistic interactions and is critical for advancing modern TCM research [7]. Strategic combination and optimal ratios of herbal pairs can enhance efficacy, reduce toxicity, or generate novel pharmacological actions [8]. *Atractylodes lancea* (Thunb.) DC. and *Atractylodis macrocephala* Koidz., both documented in the 'Shennong Materia Medica', have long been employed in the treatment of gastrointestinal disorders and possess extensive clinical usage. Modern pharmacological studies indicate that Atractylodis Rhizoma (AR) and Atractylodis Macrocephala (AM) effectively ameliorate UC symptoms [9, 10], although the mechanistic basis of the AR-AM combination in UC remains unclear.

Network pharmacology enables systematic analysis of drug-target interactions by integrating multi-omics data and constructing biological networks [11, 12]. In this study, network pharmacology was applied to predict the potential mechanisms of EEAR-AM in UC treatment. The results suggest that both the phosphatidylinositol 3-kinase (PI3K)/protein kinase B (AKT) and exchange protein directly activated by cAMP 1 (Epac1)/Ras-associated protein 1 (Rap1) signaling pathways may serve as candidate targets of EEAR-AM. Previous investigations have demonstrated that the Epac1/Rap1 pathway regulates cell adhesion and intercellular junctions. For example, the activation of this pathway has been shown to enhance endothelial barrier function by modulating Rac1 activity [13]. Importantly, activation of Epac1/Rap1 has been shown to attenuate intestinal inflammation and limit tissue injury [14].

This study integrated network pharmacology with *in vivo* and *in vitro* experiments to explore the bioactive compounds, molecular targets, and underlying pathways associated with AR-AM in UC treatment, based on the formulation described in 'Shi Jinmo Pair of Medicines'. The findings provide insights into the clinical application of the AR-AM herbal pair for UC therapy and offer a framework for investigating synergistic mechanisms in TCM formulations.

2. Materials and methods

2.1. Bioinformatics prediction of the mechanism of EEAR-AM in the treatment of UC

The active compounds in AR and AM were initially retrieved from the Traditional Chinese Medicine System Pharmacology Database (TCMSP; https://old.tcmspe.com/tcmsp.php). Compounds meeting the criteria of oral bioavailability (OB) ≥ 30% and drug-likeness (DL) ≥ 0.18 were selected as candidates for further analysis [15]. To supplement this dataset, additional active ingredients were identified using the Bioinformatics Analysis Tool for Molecular Mechanism of Traditional Chinese Medicine (Batman-TCM; http://bionet.ncpsb.org.cn/batman-tcm/). All compounds were deduplicated and integrated with previously retrieved data. Furthermore, a systematic literature review was conducted to identify any potentially overlooked bioactive constituents [16, 17].

For each selected compound, the InChI identifiers were obtained from the PubChem database (https://pubchem.ncbi.nlm.nih.gov/), and their corresponding target genes were extracted from the Batman-TCM database. Potential target genes associated with UC were collected from the GeneCards (https://www.genecards.org/) and GEO databases (https://www.ncbi.nlm.nih.gov/geo/). The GEO database provided transcriptomic data to identify differentially expressed genes associated with UC. The intersection of compound-related targets and UC-related genes was determined using Venny 2.1.0, and the resulting overlapping genes were used to generate a Venn diagram. These intersecting targets were integrated into a compound-target-disease network, constructed using Cytoscape software.

The overlapping targets between AR-AM and UC were uploaded to the STRING database (https://cn.string-db.org/) with species specified as *Homo sapiens*. A protein-protein interaction (PPI) network was constructed, and results were exported in TSV format. These data were then imported into Cytoscape to visualize the PPI network. Network topology analysis was conducted using the CytoNCA plugin. Key targets were selected based on degree centrality (DC) values greater than twice the median, along with other topological metrics exceeding their respective median values. Gene Ontology (GO) and Kyoto Encyclopedia of Genes and Genomes (KEGG) enrichment analyses were performed for the shared targets using the DAVID database (https://davidbioinformatics.nih.gov/tools.jsp), with species set to *Homo sapiens*. Data visualization was carried out using the micro-bioinformation platform (https://www.bioinformatics.com.cn/).

Molecular docking (MD) and molecular dynamics simulations were subsequently conducted. Compound structure files were obtained from PubChem, while 3D structures of key pathway proteins were retrieved from the Protein Data Bank (PDB). MD was performed using AutoDock software, and the resulting complexes were visualized with PyMOL 2.5. Molecular dynamics simulations were executed using GROMACS 2022.3 software [18, 19]. Post-simulation analyses included root-mean-square deviation (RMSD), root-mean-square fluctuation (RMSF), radius of gyration (Rg) for each amino acid residue, MMGBSA free energy calculations, and free energy landscape mapping.

2.2. In vivo experimental validation

2.2.1. Sample preparation

Dextran sodium sulfate (DSS, 160110, MP Biomedicals) solution was prepared by dissolving 3.5 g of DSS powder in 100 mL of distilled water to yield a 3.5% (*W*/*V*) solution.

Ethanolic extract of AM-AR (EEAM-AR) was prepared as follows: dried rhizomes of AM (0.3 g, batch 20220101, Hubei Tianji Pharmaceutical Co., Ltd.) and AR (0.3 g, batch 2022110103, Hubei Chenmei Traditional Chinese Medicine Co., Ltd.) were weighed, crushed, and passed through an 80-mesh sieve. The powders were combined at a 1∶1 ratio and transferred to a beaker. Ten volumes of 80% ethanol were added, and the mixture was stirred thoroughly and soaked overnight. Ultrasonic extraction was performed three times for 30 min each, with filtration after each cycle; filtrates were pooled. The combined filtrate was concentrated *via* rotary evaporation at 50 °C and 40 r·min^{-1} until a thick paste formed. The paste was transferred to a dish, covered with plastic wrap, and frozen at −80 °C overnight. Freeze-drying was conducted the following day, and the resulting extract was stored at low temperature.

Solutions of EEAR, EEAM, and EEAR-AM were prepared by accurately weighing the extracts and dissolving them in methanol to achieve a concentration of 10 mg·mL^{-1}.

A suspension of sulfasalazine (SASP, 09220718, Shanghai Xinyi Tianping Pharmaceutical Co., Ltd.) was prepared by grinding tablets into fine powder using a mortar, followed by suspension in vehicle to a final concentration of 25 mg·mL^{-1}. The suspension was aliquoted and stored at 4 °C.

2.2.2. Chromatographic and mass spectrometric conditions

Qualitative analysis of EEAR, EEAM, and EEAR-AM was performed using a ultra-high performance liquid chromatography-tandem mass spectrometry (UPLC-MS/MS) system consisting of an Agilent 1290 Infinity II liquid chromatograph and an Agilent 6460C triple quadrupole mass spectrometer (Agilent Technologies, CA, USA). Chromatographic separation was achieved using a CAPCELL PAK C18 MGIII-H column (3 μm, 2 mm × 100 mm) with a mobile phase composed of 0.1% formic acid in water (A) and acetonitrile (B). A gradient elution program was applied at a flow rate of 0.2 mL·min^{-1}: 5%–15% B from 0–5 min, 15%–55% B from 5–15 min, 55%–95% B from 15–20 min, and 95%–99% B from 20–22 min. The injection volume was 2 μL. The drying gas temperature was maintained at 350 °C with a flow rate of 9 L·min^{-1}. Capillary voltages were set at 4000 V (positive mode) and −3500 V (negative mode), and nebulizer pressure was kept at 40 psi. Data acquisition and analysis were performed using Agilent workstation software (Version B.06.00, Agilent Technologies).

2.2.3. Animals

Forty-five male BALB/c mice (SPF grade), aged 7–9 weeks and weighing 20 ± 2 g, were purchased from Liaoning Changsheng Biotechnology Co., Ltd. (Animal Production License SCXK (Liao) 2022-0003). After a 3-day acclimatization period, animals were maintained under a 12-h light/dark cycle at 22 ± 2 °C with ad libitum access to food and water. The study protocol was approved by the Animal Ethics Committee of Hubei University of Chinese Medicine (Approval No. SYXK2023-0067), ensuring compliance with ethical standards for animal research and care.

2.2.4. Experimental design

Following a 3-day acclimation period, 45 male BALB/c mice were randomly assigned to five groups (n = 9 per group): control group, model group (3.5% DSS), EEAR-AM treatment groups (555 and 1110 mg·kg^{-1}), and positive control group (SASP, 250 mg·kg^{-1}). From day 1, all groups except the control group received free access to 3.5% DSS solution for modeling, with both pure water and DSS solution refreshed every two days [20].

Pronounced weight loss and visible hematochezia in the model group confirmed successful induction of colitis. Starting on day 2, treatment groups received daily gavage with their respective doses, while the control and model groups received equivalent volumes of normal saline for 7 consecutive days. Final dosages were determined according to the latest edition of the Chinese Pharmacopoeia and prior experimental findings from our research team [16].

2.2.5. Sample collection and evaluation of disease activity index (DAI)

Body weights were recorded daily at the same time each morning [21]. Fecal occult blood tests were performed nightly to assess intestinal bleeding. During the modeling period (Table 1), average scores for weight loss, stool consistency, and hematochezia were calculated individually to determine the DAI, providing an initial assessment of model validity and therapeutic efficacy. On day 8, mice were euthanized, and colon and spleen tissues were harvested. Body weight, colon length, and spleen coefficient were measured.

Table 1 DAI scoring table.

Weight (%)	Fecal traits	Bloody stools	Score
≤ 1	Normal	Negative	0
> 1–5	semi-formed	Positive occult blood (+)	1
> 5–10	Pasty	Positive occult blood (++)	2
> 10–15	Loose stools	Gross bloody stool (+)	3
> 15	Watery stools	Gross bloody stool (++)	4

2.2.6. Histological analysis

Colon tissue from standardized anatomical regions was fixed in 4% paraformaldehyde and embedded in paraffin. Sections were subjected to hematoxylin-eosin (HE) and Alcian Blue-Periodic acid-Schiff (AB-PAS) staining. Histopathological changes were evaluated microscopically. Pathological damage scores derived from HE staining are presented in Table 2.

Table 2 Pathological impairment score.

Tissue damage	Inflammatory cell infiltration	Score
None	Infrequent	0
Isolated focal epithelial damage	Increased, some neutrophils	1
Mucosal erosions and ulcerations	Submucosal presence of inflammatory cell clusters	2
Extensive damage deep into the bowel wall	Transmural cell infiltrations	3

2.2.7. Immunohistochemical (IHC) analysis

Colon tissues were fixed in 4% paraformaldehyde, processed for paraffin embedding, deparaffinized, and subjected to antigen retrieval. Sections were incubated overnight at 4 °C with primary antibodies, followed by secondary antibody application. Immune complexes were visualized using DAB chromogen, and nuclei were counterstained with hematoxylin. Tissues were dehydrated, mounted, and examined under a microscope (Olympus, Tokyo, Japan). Primary antibodies used included MUC2 (Proteintech, 1∶1000, 27675-1-AP), matrix metalloproteinase 2 (MMP-2, Santa Cruz, 1∶200, sc-13594), and MMP-9 (Proteintech, 1∶500, 10375-2-AP).

2.2.8. Quantitative real-time polymerase chain reaction (qRT-PCR)

Colon samples were homogenized in Trizol® reagent, and total ribonucleic acid (RNA) was isolated following centrifugation steps. RNA was reverse-transcribed into cDNA according to the kit instructions. Messenger RNA (mRNA) expression levels were quantified using a StepOnePlus™ RT PCR System and PowerUp™ SYBR™ Green Master Mix, following manufacturer protocols (Vazyme Biotech, Nanjing, China). Primer sequences are listed in Supplementary Table 1. Data were analyzed using the $2^{-\Delta\Delta Ct}$ method.

2.2.9. Western blotting

Colon tissues were weighed, and protein lysates were prepared following standard protocols. Protein loading buffer was added, and samples were denatured at 100 °C for 5 min. Proteins were separated by SDS-PAGE and transferred to PVDF membranes. Membranes were incubated overnight at 4 °C with primary antibodies: MUC2 (Proteintech, 1∶1000, 27675-1-AP), zonula occludens-1 (ZO-1, Proteintech, 1∶1000, 21773-1-AP), occludin (Proteintech, 1∶1000, 27260-1-AP), claudin-1 (Proteintech, 1∶1000, 28674-1-AP), MMP-2 (Proteintech, 1∶1000, 10373-2-AP), MMP-9 (Proteintech, 1∶1000, 10375-1-AP), Epac1 (Abclonal, 1∶1000, A4149), Rap1 (Santa Cruz, 1∶300, sc-398755), PI3K (Proteintech, 1∶1000, 20584-1-AP), phosphorylated (p)-PI3K (Affinity, 1∶1000, AF4369), AKT (Pro-

teintech, 1∶1000, 10176-2-AP), and p-AKT (Proteintech, 1∶1000, 66444-1-Ig). The next day, membranes were incubated with β-actin (Abclonal, 1∶10,000, AC026) as a secondary antibody. Protein bands were detected using an ECL kit and imaged with a gel documentation system (Bio-Rad Laboratories, USA). Band intensities were quantified using ImageJ software.

2.3. *In vitro* experimental validation

2.3.1. Cell culture

Caco-2 cells were maintained in a humidified CO_2 incubator at 37 °C with 5% CO_2. Culture medium consisted of high-glucose Dulbecco's modified Eagle medium (DMEM) supplemented with 10% fetal bovine serum, 1% penicillin-streptomycin. Medium was refreshed daily, and subculturing was performed when confluence reached approximately 80%.

2.3.2. DSS concentration screening, cytotoxicity assessment, and activity evaluation

Caco-2 cells (NOBLEBIO Biotechnology, Zhejiang, China) were seeded in 96-well plates at a density of 5×10^3 cells per well. After adherence, the cells were treated with varying concentrations of EEAR-AM (0, 25, 50, 100, 200, 400 μg·mL^{-1}) for 24 h to assess cytotoxicity. Following treatment, 10 μL of cell counting kit-8 (CCK-8) reagent was added to each well and incubated for 1 h at 37 °C in a humidified atmosphere containing 5% CO_2. Absorbance was measured at 460 nm using a microplate reader. For DSS concentration screening, cells were exposed to a gradient of DSS concentrations (0.125%, 0.25%, 0.5%, 1%, 2%, 4%) to determine optimal conditions for inducing cellular stress. In the activity evaluation experiment, cells were treated with 2% DSS alone or in combination with EEAR-AM (25, 50, 100 μg·mL^{-1}). SASP (800 μg·mL^{-1}) was included as a positive control. All assays followed the same protocol as described above.

2.3.3. Experimental grouping

Caco-2 cells were divided into six groups: control, model (2% DSS), EEAR-AM treatment (25, 50, 100 μg·mL^{-1}), and positive control (SASP, 800 μg·mL^{-1}). Upon reaching the desired confluence, cells were treated as described, and mRNA and protein were harvested 24 h post-treatment for downstream analyses.

2.3.4. Intestinal barrier function assay

The effect of EEAR-AM on Caco-2 cell membrane integrity was assessed *via* transepithelial electrical resistance (TEER). A 24-well Transwell plate (Corning, NY, USA) was pre-equilibrated with DMEM in each well of a 24-well plate. Caco-2 cells were seeded at a density of 2×10^5 cells·cm^{-2} onto the apical side of Transwell inserts and cultured for 21 days. Fresh medium was replaced every other day, and cell morphology was monitored daily under a light microscope. TEER values were measured every three days using a Millicell-ERS instrument (Millipore, MA, USA) to evaluate monolayer formation and integrity [22].

A TEER value ≥ 400 Ω·cm^2 indicated successful establishment of a confluent and functional Caco-2 monolayer, suitable for further experimentation. Once stable, monolayers were randomly assigned to control, model (2% DSS), EEAR-AM (25, 50, 100 μg·mL^{-1}), or SASP (800 μg·mL^{-1}) groups. TEER measurements were recorded 24 h after treatment. TEER (Ω·cm^2) was calculated as: [Measured resistance (Ω) − background resistance (Ω)] × membrane surface area (A, cm^2), where background resistance was measured in blank inserts without cells.

2.3.5. Phalloidin staining

Caco-2 cells were seeded in 24-well plates at an appropriate density and incubated for 24 h. Cells were then randomly allocated into six groups: control, 2% DSS, EEAR-AM (25, 50, 100 μg·mL^{-1}), and SASP (800 μg·mL^{-1}). After 24 h of treatment, the culture medium was removed, and the cells were washed twice with PBS. Cells were fixed with 4% formaldehyde at room temperature, washed, and permeabilized. TRITC-conjugated phalloidin was added and incubated in the dark for 30 min at room temperature. After additional washes, a drop of anti-fade mounting medium was placed on a glass slide, and coverslips containing stained cells were mounted. Fluorescence images were captured using a fluorescence microscope.

2.3.6. QRT-PCR

mRNA expression levels of *ZO-1*, *occludin*, *claudin-1*, *tumor necrosis factor α* (*TNF-α*), *interleukin-1β* (*IL-1β*), and *IL-6* were analyzed by qRT-PCR using the same methodology as described in Section 2.2.8. Primer sequences are provided in Supplementary Table 2.

2.3.7. Western blotting assay

Protein expression was analyzed as detailed in Section 2.2.9.

2.3.8. Statistical analysis

Data were analyzed using GraphPad Prism 10.0 software (San Diego, CA, USA). Results are expressed as mean ± standard deviation (SD). Statistical significance was assessed using unpaired Student's *t*-test or one-way analysis of variance (ANOVA). For graphical representation and statistical testing, GraphPad Prism 10.0 was employed. Differences were considered statistically significant at $P < 0.05$.

3. Results

3.1. Flowcharts and TICs of EEAR-AM

The sample was processed *via* lyophilization, yielding a yellow-brown powder characterized by a fluffy texture and distinctive aroma (Fig. 1A). A qualitative analysis of EEAR, EEAM, and EEAR-AM was performed using a UPLC-MS/MS system consisting of an Agilent 1290 Infinity series liquid chromatograph coupled with an Agilent 6460C triple quadrupole mass spectrometer (Fig. 1B). Following a three-day acclimatization period with regular feeding, mice were assigned to distinct treatment groups. The control group received standard drinking water, whereas both the model and drug treatment groups were administered 3.5% DSS in their drinking water for seven days. An equivalent volume of normal saline was delivered to both the control and model groups (Fig. 1C).

3.2. EEAR-AM improved the abnormal symptoms in DSS-induced UC mice

In this study, the potential therapeutic effects of EEAR-AM were evaluated in a DSS-induced colitis model. Upon completion of the experiment, colon tissues from the DSS-treated group exhibited marked congestion and a significant reduction in length, indicating compromised colon health due to colitis. In contrast, EEAR-AM administration effectively mitigated these adverse effects associated with DSS exposure (Figs. 2A–2B). Furthermore, spleen index analysis revealed a significant increase in the model group, indicative of systemic inflammation. This elevation was notably reduced following EEAR-AM treatment, underscoring its therapeutic potential (Fig. 2C). Both EEAR-AM and SASP significantly alleviated disease-related symptoms. Additionally, both treatments suppressed the DSS-induced rise in DAI score, further supporting their beneficial roles in managing UC (Figs. 2D–2E).

Histological examination showed that colon tissue architecture in the control group remained intact, with well-formed

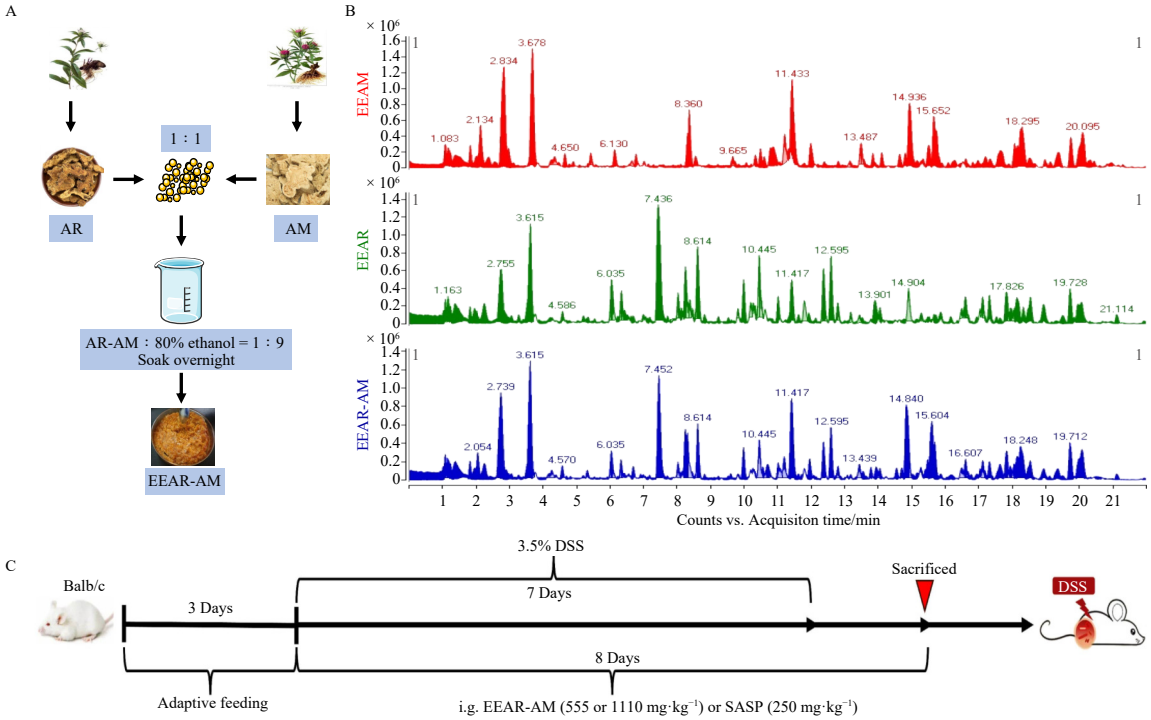

Fig. 1 (A) Flow chart for sample preparation. (B) TIC chromatograms of EEAR, EEAM, EEAR-AM using UPLC-MS/MS. (C) Development of the UC model and drug treatment as represented in experimental diagrams.

crypts and no evident epithelial erosion or ulceration. In contrast, DSS induction caused severe structural damage, inflammatory cell infiltration, and epithelial erosion or ulceration, all of which were markedly attenuated by treatment with either EEAR-AM or SASP (Figs. 2F–2G). Moreover, RT-qPCR analyses demonstrated that mRNA levels of pro-inflammatory cytokines, including *TNF-α*, *IL-1β*, and *IL-6*, were significantly upregulated in the model group. These increases were substantially reversed following EEAR-AM treatment (Figs. 2H–2J). Collectively, these findings indicate that EEAR-AM ameliorates pathological symptoms in DSS-induced UC mice.

3.3. EEAR-AM restored DSS-induced intestinal mucosal barrier function in mice

AB-PAS staining revealed impaired crypt structure and reduced goblet cell numbers in the colon tissues of the model group. However, EEAR-AM treatment led to a notable recovery in goblet cell density and reduced inflammatory cell infiltration in both the mucosa and submucosa. IHC staining further indicated that MUC2 expression in the model group was considerably lower than in the control group. Importantly, EEAR-AM treatment significantly restored MUC2 expression in colon tissues (Figs. 3A–3C). Given that E-cadherin plays a critical role in maintaining colonic epithelial barrier integrity during UC, its regulation by EEAR-AM was investigated; results are provided in Supplementary Data 1.

Additionally, the mRNA and protein levels of tight junction (TJ) proteins in colon tissues across all groups were assessed using RT-qPCR and Western blotting. The mRNA levels of *ZO-1*, *occludin*, and *claudin-1* were downregulated in the model group but showed significant upregulation after EEAR-AM treatment (Figs. 3D–3F). Western blotting results confirmed that EEAR-AM en-

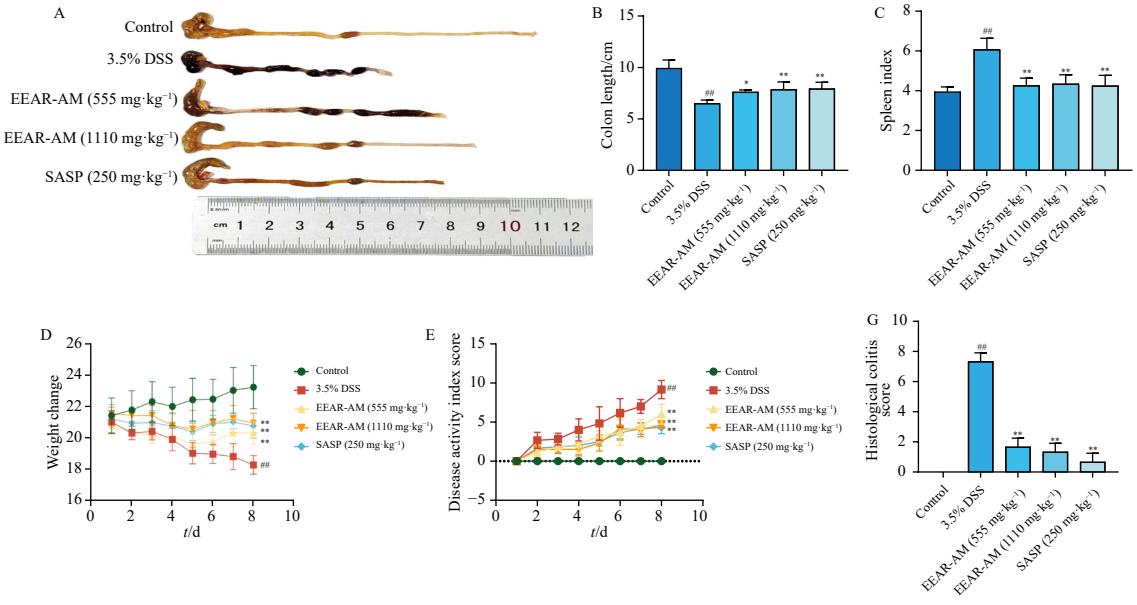

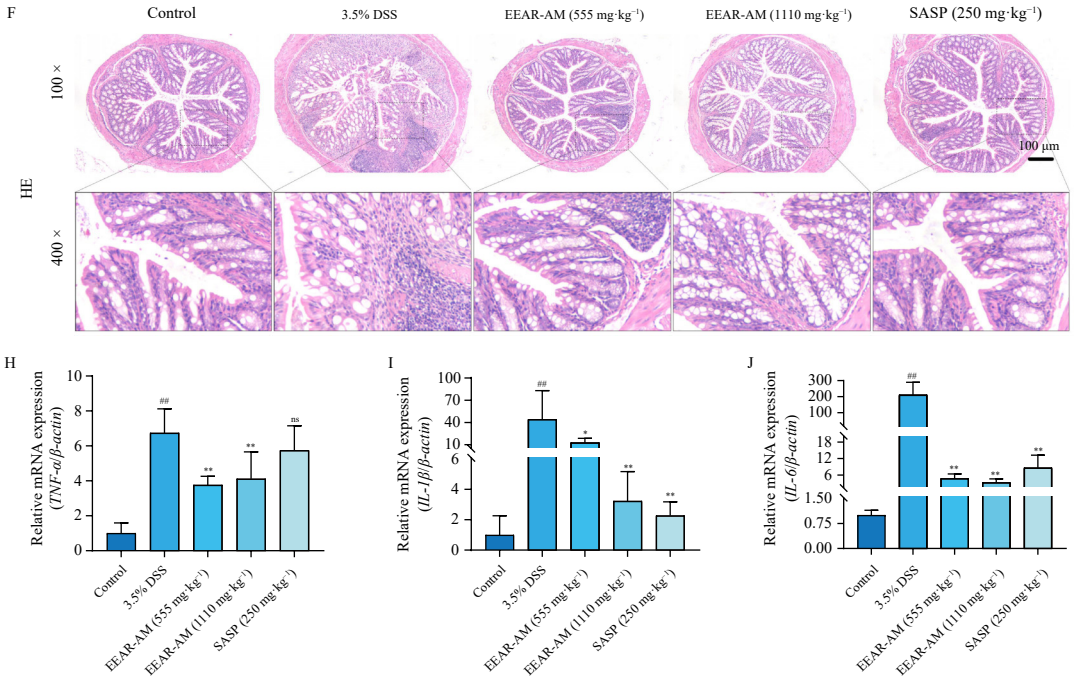

Fig. 2 Effects of EEAR-AM on symptoms in UC mice. (A) Photographs capturing the macroscopic view of the colon. (B) Statistical analysis of colon length (n = 6). (C) Spleen Index (n = 6). (D) Changes in the body weight of mice (n = 6). (E) DAI Score (n = 6). (F) HE staining images of colonic tissue (Magnification, 100 ×; Scale bar = 100 μm; n = 3). (G) Colon histopathology score. (H) Relative mRNA expression of *TNF-α*, *IL-1β* and *IL-6 (n = 3)*. The data were presented as the means ± SD. $^{\#\#}P < 0.01$ *vs* Control group; $^{*}P < 0.05$ and $^{**}P < 0.01$ *vs* 3.5% DSS group.

hanced the expression of these TJ proteins in UC mice (Figs. 3G–3K). Thus, the combined data demonstrate that EEAR-AM restores DSS-induced impairment of the intestinal mucosal barrier function.

3.4. Network pharmacological analysis of EEAR-AM in the treatment of UC

Differentially expressed genes from the GSE38713,

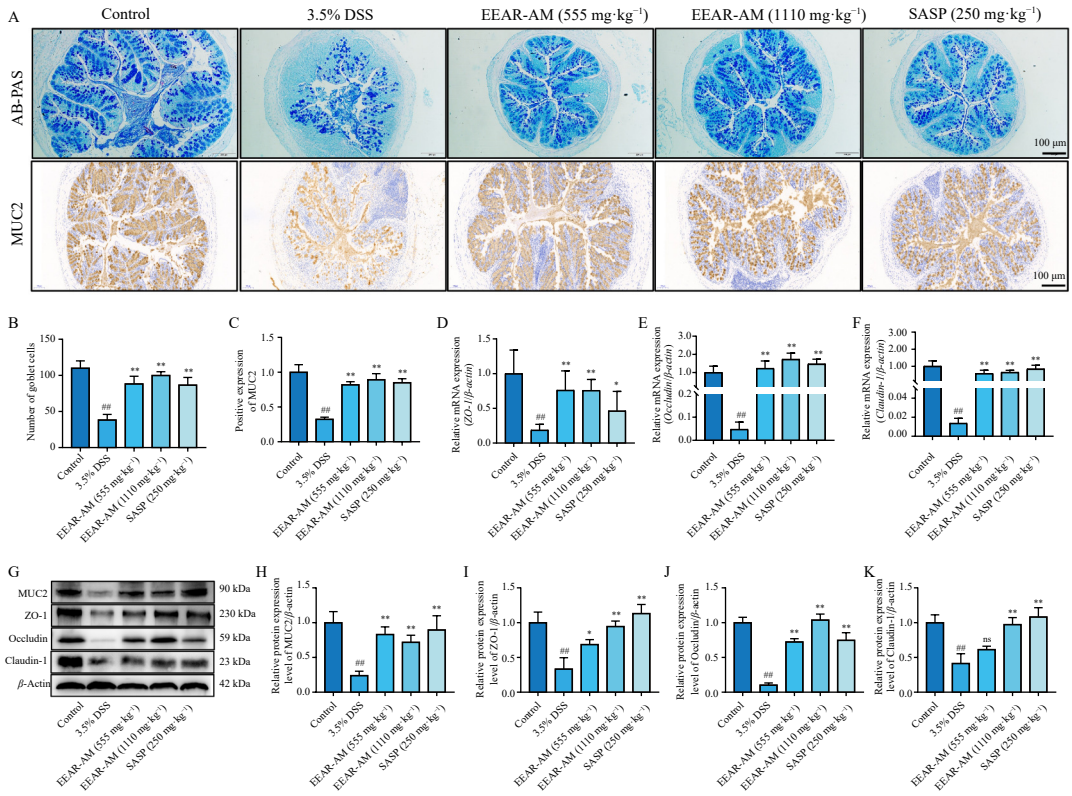

Fig. 3 Effects of EEAR-AM on the expressions of MUC2 and TJ proteins in UC mice. (A) AB-PAS staining and expression levels of MUC2 in colon tissues were examined by IHC staining (Magnification, 100 ×; scale bar = 100 μm). (B) Chart of goblet cell count. (C) Statistical chart of IHC results of expression levels of MUC2. (D–F) The mRNA levels of *ZO-1*, *Occludin,* and *Claudin-1* in colon were detected by RT-PCR. (G) Expression levels of MUC2, ZO-1, Occludin, and Claudin-1 in colon tissues were detected by Western blotting. (H–K) The gray intensity analysis of MUC2, ZO-1, Occludin, and Claudin-1. The data were presented as the means ± SD (n = 3); $^{\#\#}P < 0.01$ *vs* Control group; $^{*}P < 0.05$ and $^{**}P < 0.01$ *vs* 3.5% DSS group.

GSE59071, and GSE87466 datasets in the GEO database were visualized as volcano plots (Fig. 4A). Using the TCMSP and Batman-TCM databases, 36 active ingredients were identified, including 23 linked to AR, 9 to AM, and 4 shared components. From Batman-TCM, 886 targets associated with AR-AM active ingredients were extracted. Concurrently, the GeneCards and GEO databases identified 5,158 UC-related targets. Analysis revealed 435 overlapping targets between active ingredient targets and UC-related targets (Fig. 4B). A "drug-component-disease-target" network diagram comprising 466 nodes and 1,316 edges was constructed, illustrating 435 common targets connected to 35 active ingredients, with color and shape encoding categorical distinctions (Fig. 4C). Key components in EEAR-AM were verified using liquid chromatography-mass spectrometry (LC-MS), with identification results for six major active ingredients detailed in Supplementary Data 2. Core targets were screened using the MCC algorithm in cytohubba (a Cytoscape plugin), identifying HIF1A, AKT1, TP53, and others as top-ranking proteins (Fig. 4D). Enrichment analysis suggested that EEAR-AM may exert its effects through processes such as protein phosphorylation, plasma membrane localization, and protein tyrosine kinase activity (Fig. 4E). KEGG pathway enrichment analysis, following the exclusion of pathways unrelated to UC, identified the top 10 signaling pathways ranked by p-value. These were visualized as bubble plots (Fig. 4F), with the PI3K/AKT and Rap1 signaling pathways emerging as key contributors to the therapeutic mechanism of EEAR-AM.

3.5. Strong binding activity between active compounds and targets

MD and molecular dynamics simulations were conducted to evaluate the binding interactions between active compounds and target proteins. Heatmap analysis of docking scores revealed notably strong affinities, particularly between PI3K and atractylolide I and between Rap1 and atractylolide II, with the latter interaction shown in detail (Figs. 5A–5C). Subsequent MD simulations confirmed the stability of these complexes. Key dynamic parameters, RMSD, RMSF, solvent-accessible surface area (SASA), Rg, and binding energy, remained within acceptable ranges throughout the simulation period (Figs. 5D–5H).

3.6. EEAR-AM inhibited the expression of MMP-2 and MMP-9 in DSS-induced UC mice

The results obtained from IHC staining indicated that EEAR-AM notably reduced the levels of MMP-2 and MMP-9 in mice with UC (Figs. 6A–6C). Moreover, RT-qPCR analysis revealed that the mRNA levels of *MMP-2* and *MMP-9* were significantly elevated in

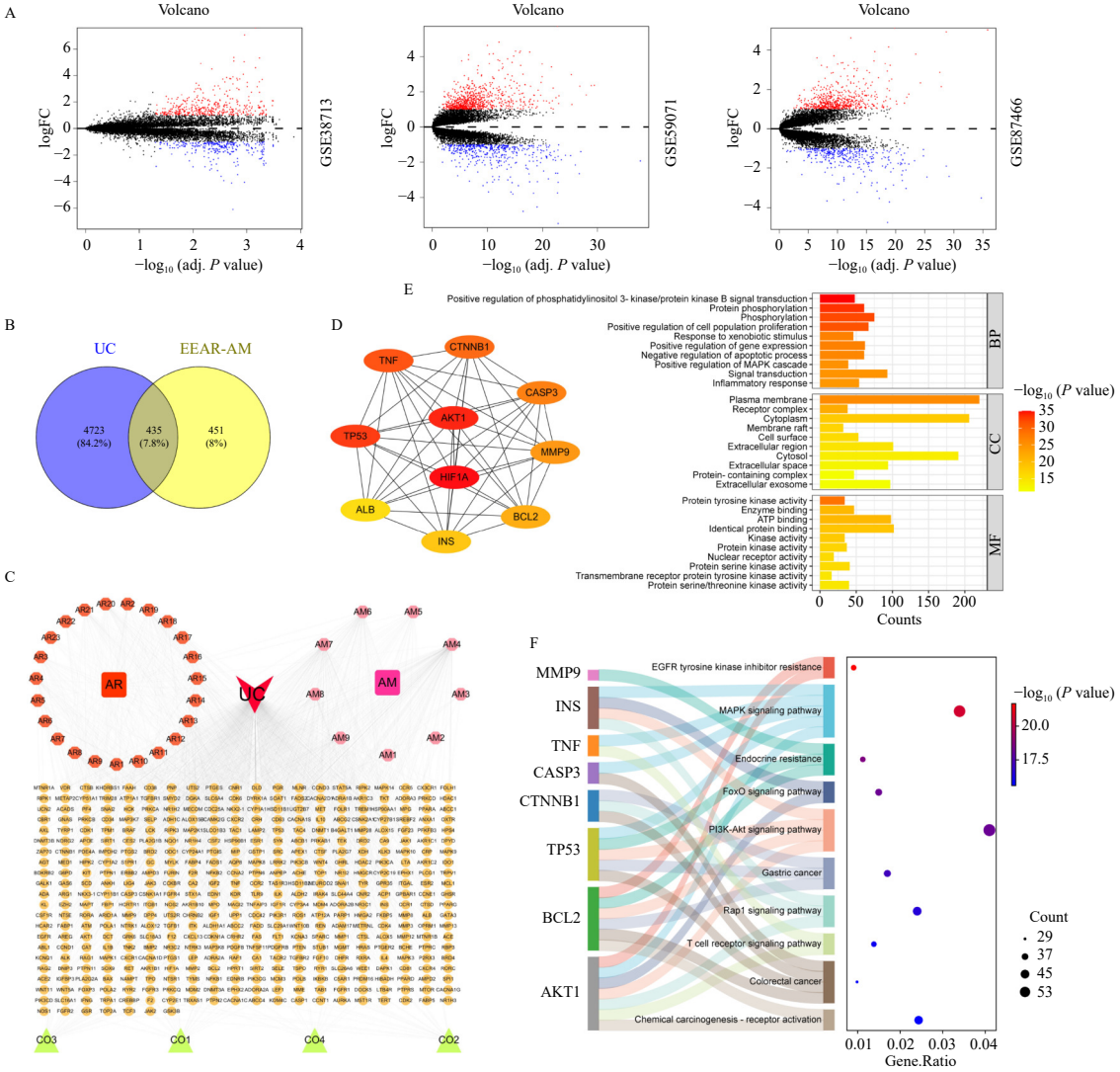

Fig. 4 Network pharmacological analysis of EEAR-AM in the treatment of UC. (A) Volcanograms of differential genes for GSE38713, GSE59071, and GSE87466, respectively (up: red, down: blue). (B) Venn Diagram. (C) TCM-component-target-disease network diagram. (D) PPI network diagram of EEAR-AM in the treatment of UC. (E) GO enrichment analysis. (F) KEGG enrichment analysis.

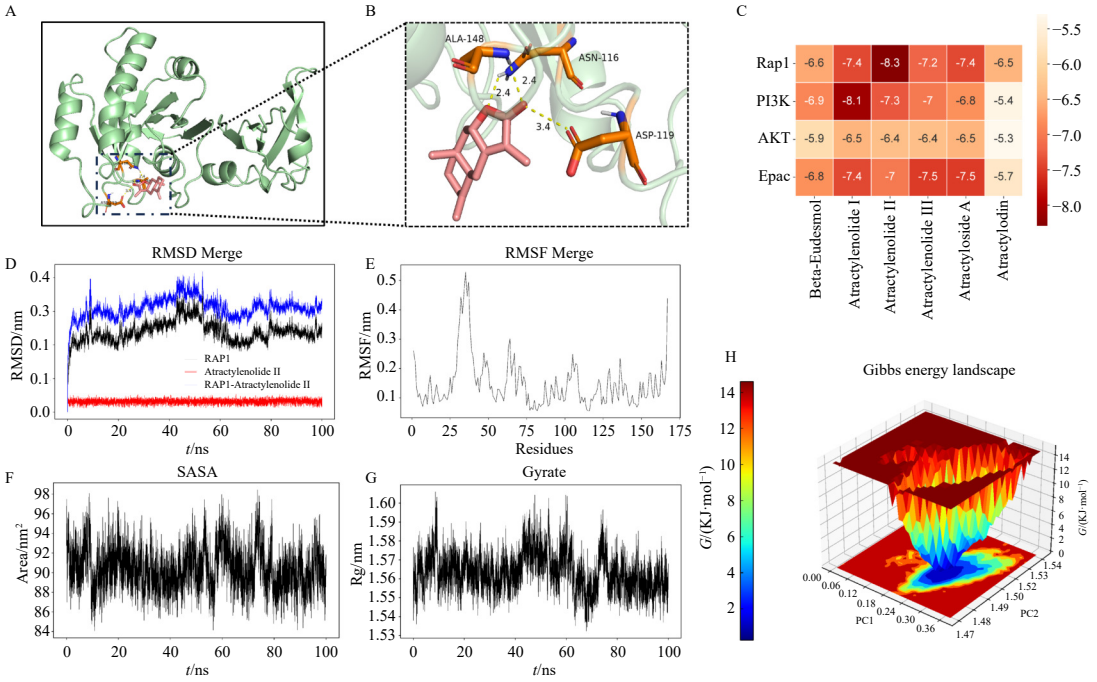

Fig. 5 Molecular docking and dynamics simulation reveal strong binding interactions between active compounds and target proteins. (A–B) Molecular docking visualization. (C) Molecular docking heat map. (D) RMSD profile of the Rap1-atractylolactone II complex. (E) RMSF analysis of the Rap1-atractylolactone II complex. (F) SASA of the Rap1-atractylolactone II complex. (G) Radius of gyration (Rg) analysis of the Rap1-atractylolactone II complex. (H) Three-dimensional energy landscape (free energy topography).

the model group compared to the control group, whereas treatment with EEAR-AM led to a marked reduction in these mRNA levels (Figs. 6D–6E). Furthermore, Western blotting results corroborated these findings. Collectively, these data indicate that EEAR-AM has the potential to inhibit the expression of MMP-2 and MMP-9 in DSS-induced UC mice.

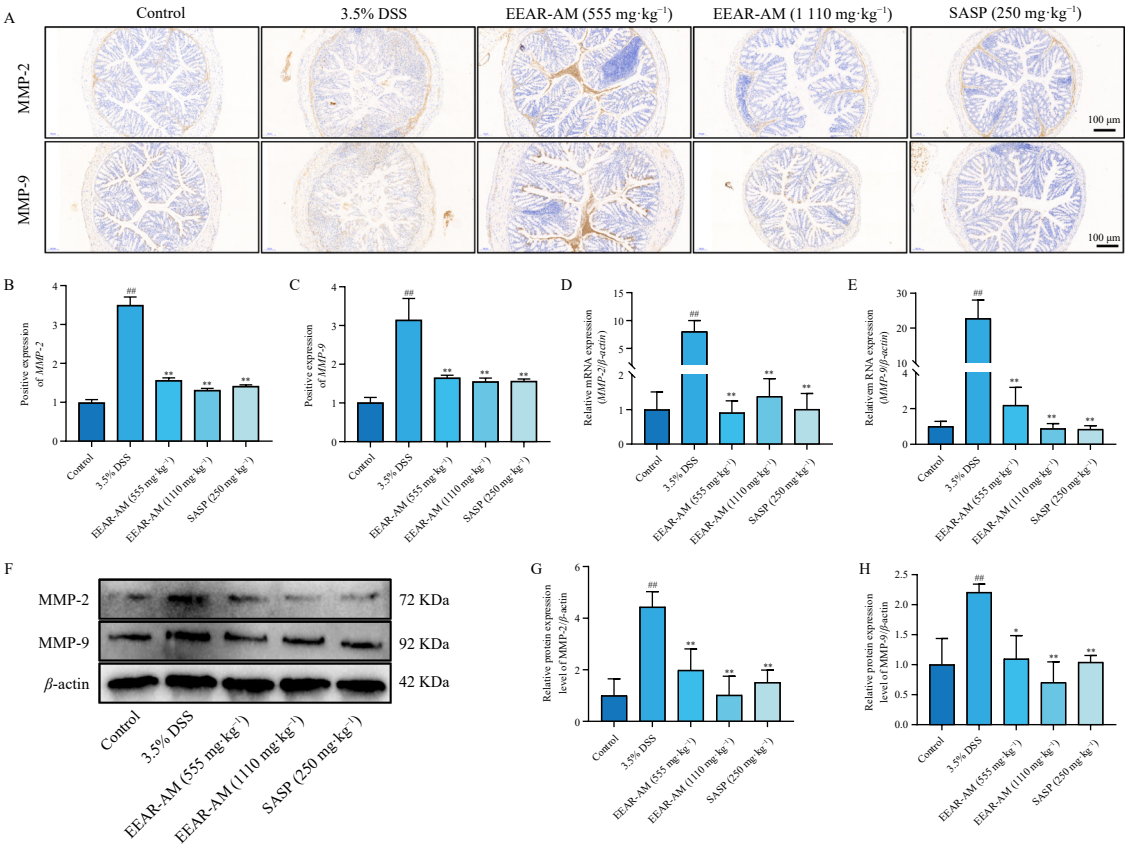

Fig. 6 Effects of EEAR-AM on the expressions of MMP-2/9 in UC mice. (A) Expressions levels of MMP-2 and MMP-9 in colon tissues were detected by IHC (Magnification, 100 ×; scale bar = 100 μm). (B–C) Relative positive expressions area analysis of MMP-2 and MMP-9. (D–E) The mRNA levels of *MMP-2* and *MMP-9* in colon tissues. (F) Expressions levels of MMP-2 an d MMP-9 in colon tissues were detected by Western blotting. (G–H) The gray intensity analysis of MMP-2 and MMP-9. The data were presented as the means ± SD (n = 3); $^{\#\#}P < 0.01$ *vs* Control group; $^{*}P < 0.05$ and $^{**}P < 0.01$ *vs* 3.5% DSS group.

3.7. EEAR-AM regulated the Epac1/Rap1 and PI3K/AKT pathways in DSS-induced UC mice

Building on our prior network pharmacology predictions, we used Western blotting to examine how EEAR-AM modulates the Epac1/Rap1 and PI3K/AKT pathways in DSS-induced UC mice. Compared to the control group, the model group exhibited significantly decreased protein levels of Epac1 and Rap1, while phosphorylation levels of PI3K and AKT were markedly increased. In contrast, both the EEAR-AM and SASP groups showed reversal of these alterations (Fig. 7). These results suggest that EEAR-AM may alleviate UC symptoms by activating the Epac1/Rap1 pathway and suppressing the PI3K/AKT pathway.

3.8. EEAR-AM improved cell monolayer injury in DSS-induced Caco-2 cells

The optimal concentrations of DSS and EEAR-AM were determined using the CCK-8 assay. Following the manufacturer's protocol, 2% DSS was identified as the appropriate concentration to induce cellular injury without excessive cytotoxicity (Fig. 8A). Additionally, EEAR-AM at concentrations up to 100 μg·mL^{-1} showed no significant toxicity to Caco-2 cells, leading to the selection of 2 % DSS in combination with EEAR-AM at 25, 50, and 100 μg·mL^{-1} for subsequent experiments (Fig. 8B). The protective effects of EEAR-AM against DSS-induced injury in Caco-2 cells were also assessed using the CCK-8 method. The results demonstrated that EEAR-AM (25, 50, and 100 μg·mL^{-1}) significantly attenuated cell injury (Fig. 8C).

Transendothelial electrical resistance (TEER) values increased progressively over time, and a stable cell monolayer barrier model was established when TEER reached or exceeded 400 Ω·cm^2. The model group exhibited significantly lower TEER values than the control group, whereas both EEAR-AM and SASP effectively prevented this decline. These findings suggest that EEAR-AM can ameliorate DSS-induced intestinal epithelial barrier dysfunction in Caco-2 monolayers by enhancing TEER and reducing paracellular permeability (Figs. 8D–8E). Finally, RT-qPCR analyses revealed that EEAR-AM (25, 50, and 100 μg·mL^{-1}) suppressed the DSS-induced inflammatory response in Caco-2 cells, as evidenced by significant reductions in the mRNA levels of *TNF-α*, *IL-1β*, and *IL-6* compared to the model group (Figs. 8F–8H).

3.9. EEAR-AM ameliorated intestinal epithelial barrier dysfunction in DSS-induced Caco-2 cells

Immunofluorescence assays showed a notable increase in F-actin expression following EEAR-AM treatment, suggesting that EEAR-AM contributes to colonic protection by stabilizing the actin cytoskeleton (Fig. 9A). RT-qPCR and Western blotting analyses further demonstrated that EEAR-AM increased the mRNA and protein levels of TJ proteins ZO-1, occludin, and claudin-1 in DSS-induced Caco-2 cells (Figs. 9B–9H). Additionally, Western blotting results showed that DSS treatment significantly upregulated MMP-2 and MMP-9 protein expression, whereas both EEAR-AM and SASP markedly reduced their expression levels (Figs. 9I–9K).

3.10. EEAR-AM regulated the Epac1/Rap1 and PI3K/AKT pathways in DSS-induced Caco-2 cells

The Western blotting analysis revealed a significant decrease in Epac1 and Rap1 protein levels in the model group. Conversely, the expression levels of p-PI3K and p-AKT proteins were markedly elevated. However, EEAR-AM effectively counteracted these aberrant changes in protein expression. These findings indicate that EEAR-AM protects against DSS-induced injury in Caco-2 cells by activating the Epac1/Rap1 signaling pathway and simultaneously suppressing the PI3K/AKT pathway (Figs. 10A–10F).

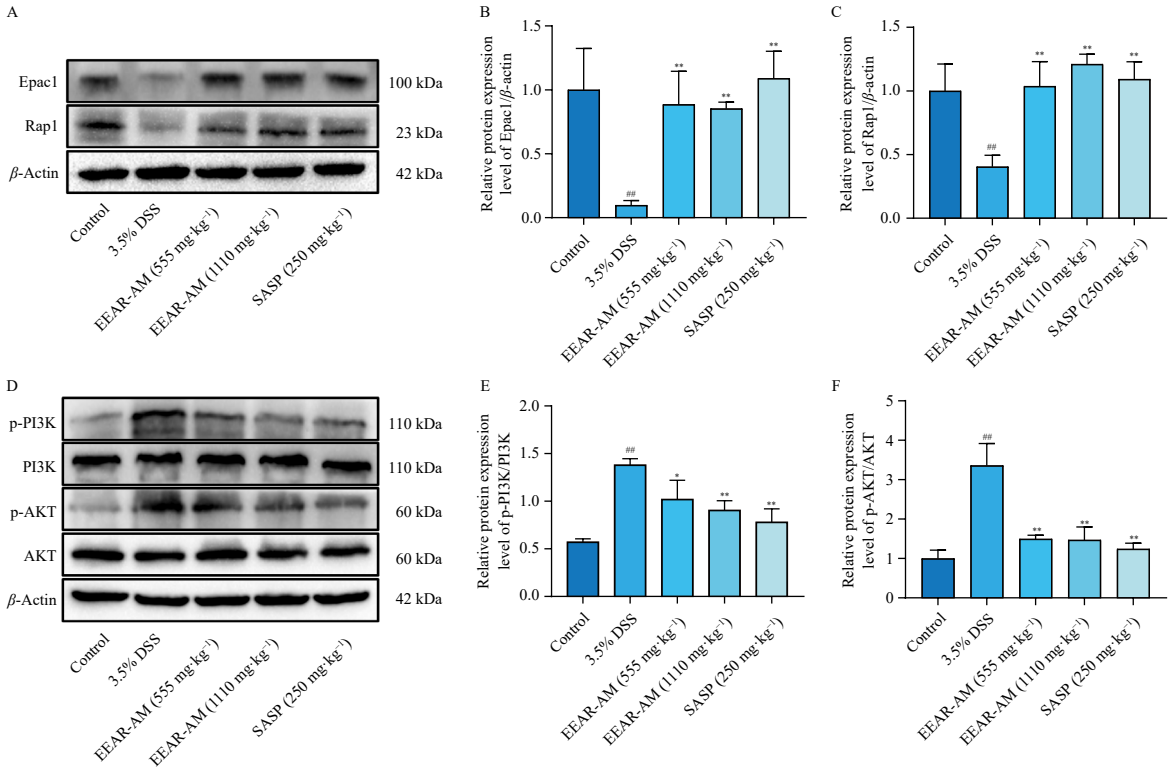

Fig. 7 Effects of EEAR-AM on the regulation of Epac1/Rap1 and PI3K/AKT pathways in UC mice. (A) Expression levels of Epac1/Rap pathway-related proteins were detected by Western blotting. (B–C) The gray intensity analysis of Epac1 and Rap1 proteins. (D) Expression levels of PI3K/AKT pathway-related proteins were detected by Western blotting. (E–F) The gray intensity analysis of p-PI3K/PI3K and p-AKT/AKT. The data were presented as the means ± SD (n = 3). $^{\#\#}P < 0.01$ *vs* Control group; $^{*}P < 0.05$ and $^{**}P < 0.01$ *vs* 3.5 % DSS group.

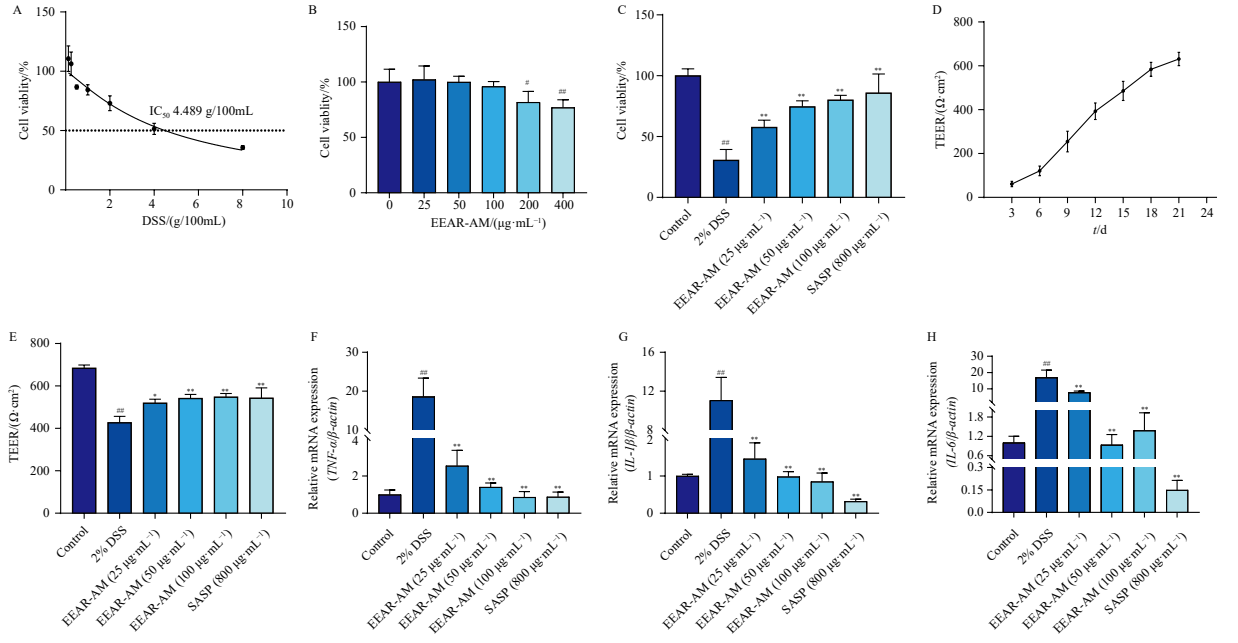

Fig. 8 Effects of EEAR-AM on cell injury and inflammation in DSS-induced Caco-2 cells. (A) Cell viability of Caco-2 after 24 h treatment with different concentrations of DSS. (B) Cell viability of Caco-2 after 24 h of EEAR-AM treatment (n = 6). (C) Caco-2 cell viability after 24 h treatment with 2 % DSS and different concentrations of EEAR-AM (n = 6). (D) Caco-2 cells monolayer construction. (E) TEER value after EEAR-AM administration (n = 6). (F–H) The mRNA levels of *TNF-α*, *IL-1β*, and *IL-6* in DSS-induced Caco-2 cells (n = 3). The data were presented as the means ± SD. $^{\#\#}P < 0.01$ *vs* Control group; $^{*}P < 0.05$ and $^{**}P < 0.01$ *vs* 2% DSS group.

4. Discussion

In recent years, although the fundamental mechanisms underlying UC remain unclear, extensive and ongoing research into its pathogenesis has emphasized the intestinal mucosal barrier as a critical focal point. This barrier consists of four essential components: mechanical, chemical, immune, and biological barriers. Among these, the mechanical barrier constitutes the primary structure of the intestinal mucosal barrier and serves as the first line of defense against the invasion of external pathogenic microorganisms [23].

The intestinal mechanical barrier is primarily composed of intestinal epithelial cells, TJs between these cells, and the extracellular mucus layer coating the gut lining [24]. Specific types of intestinal epithelial cells, including goblet and Paneth cells, play critical roles in maintaining the physical integrity of the gut barrier. These specialized cells undergo continuous renewal, a process mediated by intestinal epithelial stem cells located at the base of the crypts. These stem cells contribute not only to epithelial regeneration but also to mucus production, which protects the intestinal mucosa [25]. In addition, intestinal epithelial cells have evolved specialized mechanisms to sense and respond to external stimuli, which are critical for initiating and regulating appropriate immune responses within the gastrointestinal tract. Another study has shown that alterations in actin dynamics inhibit cell cycle progression, increase apoptosis, and reduce colonic epithelial cell proliferation, thereby exacerbating the development and progression of colitis [26].

Research demonstrates that downregulation of TJ proteins, including claudin-1 and occludin, impairs the mechanical barrier and increases intestinal permeability. This disruption triggers immune activation and promotes inflammatory cell infiltration [27]. Furthermore, the release of pro-inflammatory cytokines is not only crucial in UC pathogenesis but also serves as a key indicator

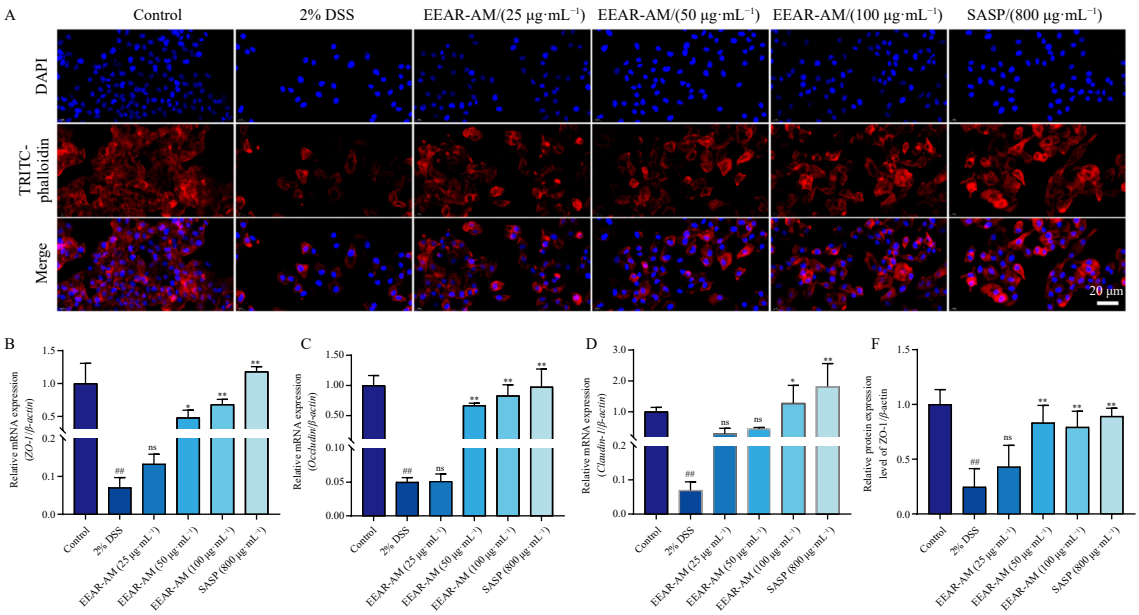

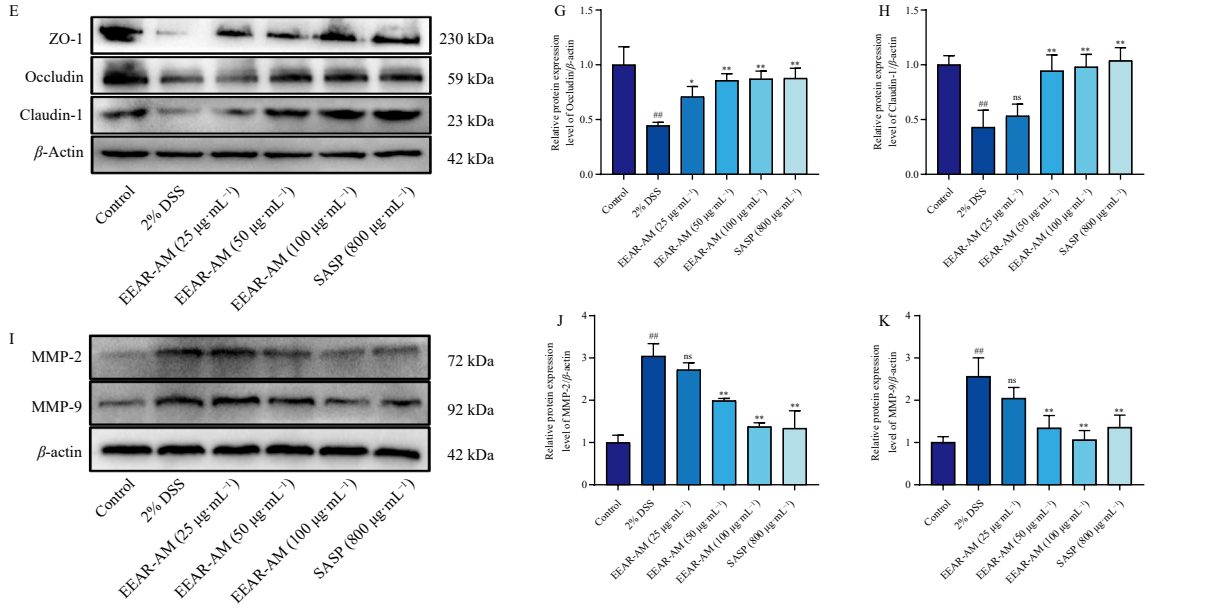

Fig. 9 Effects of EEAR on the expressions of TJ proteins and MMP-2/9 in DSS-induced Caco-2 cells. (A) Phalloidin staining. (B–D) The mRNA levels of *ZO-1*, *Occludin* and *Claudin-1* were detected by RT-PCR. (E) Expression levels of ZO-1, Occludin, and Claudin-1 proteins were detected by Western blotting; (F–H) The gray intensity analysis of ZO-1, Occludin, and Claudin-1 proteins. (I) Expression levels of MMP-2 and MMP-9 proteins were detected by Western blotting. (J–K) The gray intensity analysis of MMP-2 and MMP-9 proteins. The data were presented as the means ± SD (n = 3) ; $^{\#\#}P < 0.01$ *vs* Control group; $^{*}P < 0.05$ and $^{**}P < 0.01$ *vs* 2% DSS group.

of inflammatory intensity [28]. To evaluate the effects of EEAR-AM on mucosal recovery and inflammation reduction in UC, we assessed pro-inflammatory cytokines such as TNF-α, IL-6, and IL-1β. Additionally, this study focused on TJ proteins and goblet cell populations to investigate the reparative effects of EEAR-AM on UC-affected intestinal mucosa. The findings revealed that EEAR-AM significantly attenuated weight loss, spleen enlargement, colon shortening, and DAI scores, while suppressing mRNA expression of *TNF-α*, *IL-6*, and *IL-1β* in UC mice. Moreover, EEAR-AM increased both mRNA and protein levels of ZO-1, occludin, and claudin-1. Histopathological evaluation indicated that colon tissue architecture in the EEAR-AM group was better preserved, with markedly reduced inflammatory cell infiltration and increased goblet cell numbers compared to the model group.

IHC analysis demonstrated a significant increase in mucin MUC2 expression and a marked decrease in MMP-2 and MMP-9 levels relative to the model group. Western blotting results from

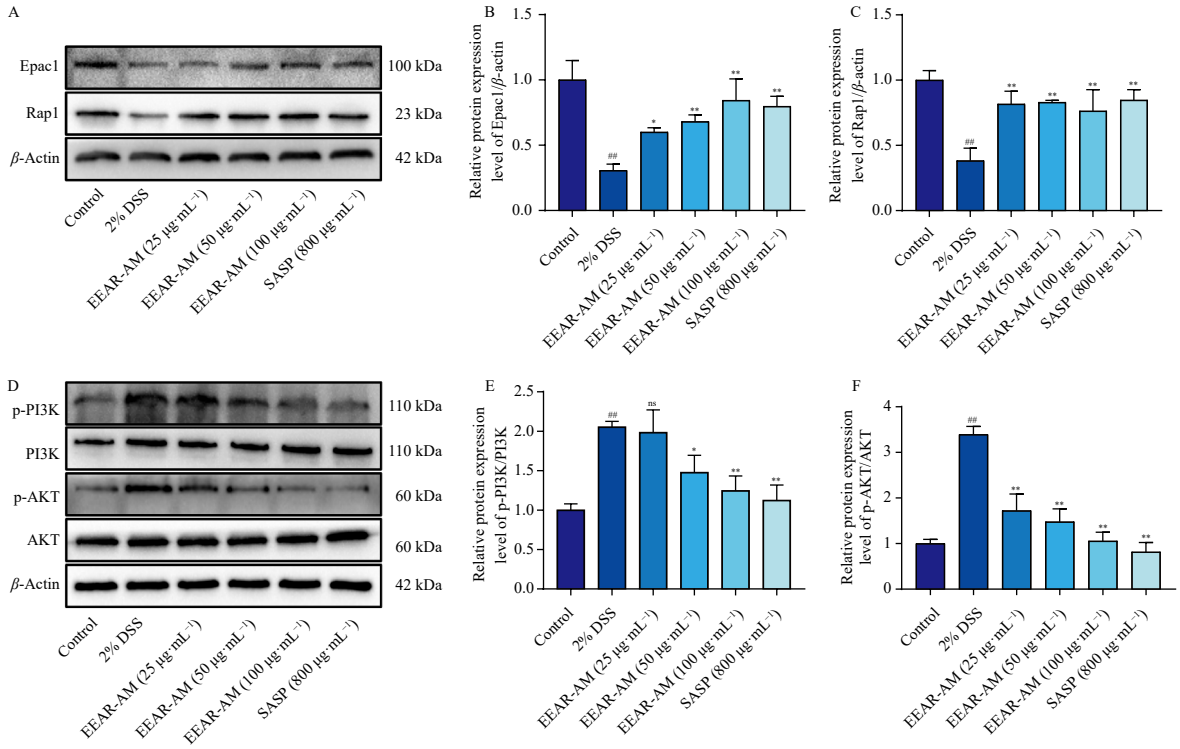

Fig. 10 Effects of EEAR-AM on the regulation of Epac1/Rap1 and PI3K/AKT pathway in DSS-induced Caco-2 cells. (A) Expression levels of Epac1/Rap pathway-related proteins were detected by Western blotting. (B–C) The gray intensity analysis of Epac1 and Rap1 proteins. (D) Expression levels of PI3K/AKT pathway-related proteins were detected by Western blotting. (E–F) The gray intensity analysis of p-PI3K/PI3K and p-AKT/AKT. The data were presented as the means ± SD (n = 3); $^{\#\#}P < 0.01$ *vs* Control group; $^{*}P < 0.05$ and $^{**}P < 0.01$ *vs* 2% DSS group.

both *in vitro* and *in vivo* experiments showed that TJ protein levels in the model group were significantly lower than those in the control group, with a notable restoration following EEAR-AM treatment. The expression patterns of MMP-2 and MMP-9 proteins were consistent with IHC findings. However, the precise mechanisms by which EEAR-AM ameliorates UC-related impairment of the intestinal mucosal barrier require further investigation.

Using network pharmacology, this study explored the mechanisms through which EEAR-AM improves UC, substantiating these mechanisms *via* both *in vitro* and *in vivo* investigations. A comprehensive database search and literature review identified 35 potential active compounds in EEAR-AM for UC treatment, including atractylolactone I, II, and III, atractylodin, and *β*-eudesmol, many of which exhibit anti-inflammatory properties. Recent studies indicate that atractylenolide I possesses significant anti-inflammatory activity; it alleviates UC symptoms by downregulating genes involved in fructose and galactose metabolism (including SPHK1 and B4GALT2), thereby reducing PI3K/AKT signaling pathway activation [9]. Atractylolactone II attenuates the effects of the lncRNA XIST/miR-30a-5p/ROR1 pathway in colorectal cancer cells, leading to decreased proliferation and viability [29]. Similarly, atractylenolide III exerts notable anti-inflammatory effects, improving intestinal epithelial barrier function and mitigating mitochondrial dysfunction through activation of the AMPK/SIRT1/PGC-1α pathway, which helps prevent UC exacerbation [30]. Atractylodin demonstrates potent anti-inflammatory effects in UC treatment [31], acting *via* PPARα-dependent pathways [32].

Furthermore, studies have indicated that polysaccharide constituents from AR and AM exert significant protective effects against UC. Specifically, AM-derived polysaccharides modulate the Th17/Treg cell balance by inhibiting the IL-6/STAT3 pathway, contributing to UC management [33]. Additionally, AM polysaccharides improve UC outcomes by significantly reducing levels of harmful bacteria such as *Clostridium* sensu stricto 1 and *Escherichia-Shigella*, while promoting beneficial strains including *Faecalibaculum* and *Bifidobacterium* [34]. Likewise, AR-derived polysaccharides help restore gut microbiota equilibrium in mice by increasing the relative abundance of *Lactobacillus* and *Faecalibaculum*, a mechanism critical for protecting the intestinal mucosal barrier and enhancing mucosal immunity [12]. These findings collectively underscore the anti-inflammatory properties of EEAR-AM's active components, supporting its potential efficacy in UC treatment.

KEGG pathway enrichment analysis revealed significant involvement of the MAPK, Rap1, and PI3K/AKT pathways. Among these, Rap1, a member of the Ras family of small GTPases, can activate downstream targets and regulate multiple signaling cascades, including the PI3K/AKT pathway. These pathways are widely expressed across tissue types and are vital for diverse biological processes such as cell proliferation, polarity formation, differentiation, adhesion, and vascular remodeling [35, 36]. Evidence suggests that the Epac1/Rap1 pathway primarily regulates cell adhesion and intercellular junctions [37]. This pathway is closely associated with UC, and its activation enhances Epac1 and Rap1 expression in inflamed colon tissues, contributing to improved colonic pathology and repair of intestinal mucosal damage [14]. Similarly, the PI3K/Akt signaling pathway plays a pivotal role in UC progression and intestinal injury exacerbation [14]. Similarly, the PI3K/Akt signaling pathway plays a vital role in both the progression of UC and the exacerbation of intestinal injury [38]. During chronic inflammation, hyperactivation of this pathway may lead to abnormal tissue growth and initiate carcinogenic mechanisms linked to UC [39]. Our study indicates that EEAR-AM may promote intestinal mucosal healing in UC by activating the Epac1/Rap1 pathway while simultaneously suppressing the PI3K/AKT pathway, as demonstrated in both *in vitro* and *in vivo* experiments (Fig. 11).

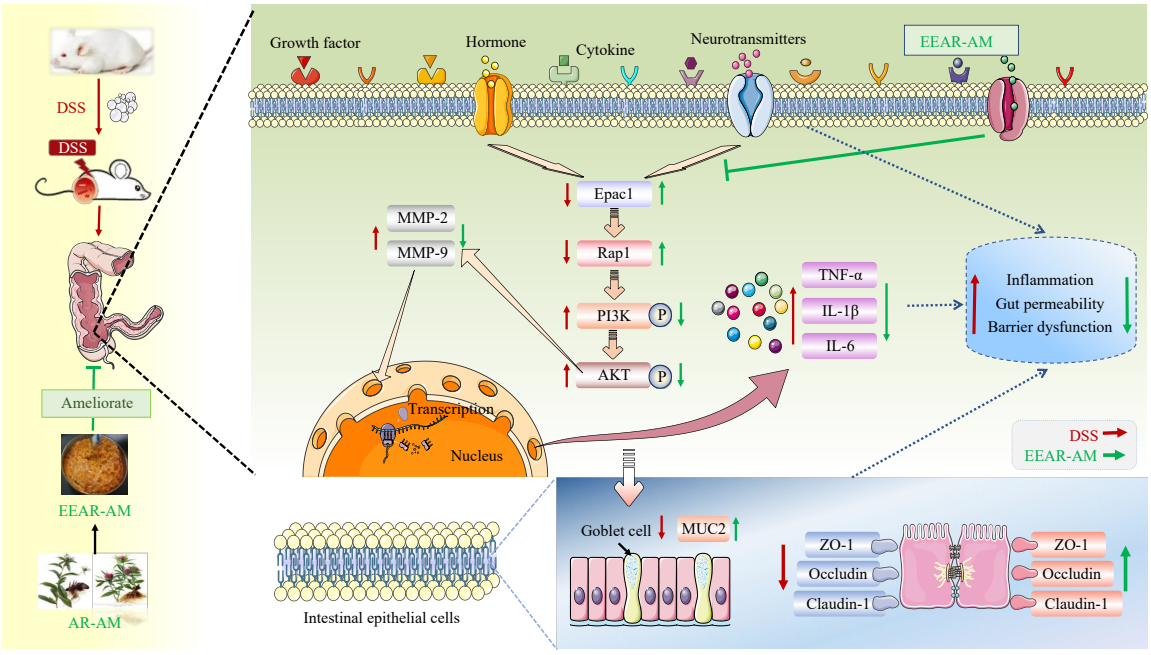

Fig. 11 Proposed mechanism of EEAR-AM in protecting intestinal barrier integrity in UC. DSS treatment activates the Epac1/Rap1 signaling pathway, which subsequently stimulates the PI3K/AKT pathway. This activation leads to upregulated expression of MMP-2/9 proteins, which degrade tight junction (TJ) proteins, thereby compromising intercellular junctions and disrupting the integrity of the intestinal epithelial barrier. As a result, intestinal mucosal barrier function is impaired. In contrast, EEAR-AM ameliorates intestinal mucosal injury by activating the Epac1/Rap1 pathway while concurrently inhibiting the PI3K/AKT signaling cascade.

This study provides new insights into EEAR-AM-mediated restoration of the intestinal barrier in UC. However, several limitations warrant further investigation. First, identifying the most influential bioactive components within EEAR-AM remains challenging due to its complex composition. Second, direct experimental evidence confirming the regulatory effects of EEAR-AM on the Epac1/Rap1 and PI3K/AKT pathways is currently limited. Finally, additional signaling pathways identified in the enrich-

ment analysis require further experimental validation in future studies.

5. Conclusion

In summary, findings from both *in vivo* and *in vitro* experiments indicate that EEAR-AM promotes the repair of intestinal mucosal injury and facilitates the restoration of intestinal barrier integrity. These protective effects may be mediated, at least in part, by the activation of the Epac1/Rap1 pathway and concurrent inhibition of the PI3K/AKT pathway.

Funding

This work was supported by the Key Scientific ResearchProject of Hubei Provincial Department of Education (No. D20232001).

Supporting information

Supporting materials of this paper can be requested by sending E-mail to the corresponding authors.

Declaration of competing interest

The authors declare that they have no conflicts of interest.

References

1 Chen Y, Liang J, Chen S, et al. Discovery of vitexin as a novel VDR agonist that mitigates the transition from chronic intestinal inflammation to colorectal cancer. *Mol Cancer*. 2024;23(1):196. https://doi.org/10.1186/s12943-024-02108-6.
2 Xu R, Du A, Deng X, et al. tsRNA-GlyGCC promotes colorectal cancer progression and 5-FU resistance by regulating SPIB. *J Exp Clin Cancer Res*. 2024;43(1):230. https://doi.org/10.1186/s13046-024-03132-6.
3 Gros B, Kaplan GG. Ulcerative colitis in adults: a review. *JAMA*. 2023;330(10):951-965. https://doi.org/10.1001/jama.2023.15389.
4 Turner JR. Intestinal mucosal barrier function in health and disease. *Nat Rev Immunol*. 2009;9(11):799-809. https://doi.org/10.1038/nri2653.
5 Kaminsky LW, Al-Sadi R, Ma TY. IL-1β and the intestinal epithelial tight junction barrier. *Front Immunol*. 2021;12:767456. https://doi.org/10.3389/fimmu.2021.767456.
6 Zong Y, Meng J, Mao T, et al. Repairing the intestinal mucosal barrier of traditional Chinese medicine for ulcerative colitis: a review. *Front Pharmacol*. 2023;14:1273407. https://doi.org/10.3389/fphar.2023.1273407.
7 Liu X, Lv M, Wang Y, et al. Deciphering the compatibility rules of traditional Chinese medicine prescriptions based on NMR metabolomics: a case study of Xiaoyaosan. *J Ethnopharmacol*. 2020;254:112726. https://doi.org/10.1016/j.jep.2020.112726.
8 Lin L, Zhou X, Gao T, et al. Herb pairs containing Curcumae Rhizoma (Ezhu): a review of bio-active constituents, compatibility effects and t-copula function analysis. *J Ethnopharmacol*. 2024,319(Pt 3):117199. https://doi.org/10.1016/j.jep.2023.117199.
9 Qu L, Liu C, Ke C, et al. *Atractylodes lancea* rhizoma attenuates DSS-induced colitis by regulating intestinal flora and metabolites. *Am J Chin Med*. 2022;50(2):525-552. https://doi.org/10.1142/S0192415X22500203.
10 Cheng H, Zhang D, Wu J, et al. *Atractylodes macrocephala* Koidz. volatile oil relieves acute ulcerative colitis via regulating gut microbiota and gut microbiota metabolism. *Front Immunol*. 2023;14:1127785. https://doi.org/10.3389/fimmu.2023.1127785.
11 Zhao L, Zhang H, Li N, et al. Network pharmacology, a promising approach to reveal the pharmacology mechanism of Chinese medicine formula. *J Ethnopharmacol*. 2023;309:116306. https://doi.org/10.1016/j.jep.2023.116306.
12 Wang YX, Yang Z, Wang WX, et al. Methodology of network pharmacology for research on Chinese herbal medicine against COVID-19: a review. *J Integr Med*. 2022;20(6):477-487. https://doi.org/10.1016/j.joim.2022.09.004.
13 Aslam M, Tanislav C, Troidl C, et al. cAMP controls the restoration of endothelial barrier function after thrombin-induced hyperpermeability *via* Rac1 activation. *Physiol Rep*. 2014;2(10):e12175. https://doi.org/10.14814/phy2.12175.
14 Li H, Fan C, Feng C, et al. Inhibition of phosphodiesterase-4 attenuates murine ulcerative colitis through interference with mucosal immunity. *Br J Pharmacol*. 2019;176(13):2209-2226. https://doi.org/10.1111/bph.14667.
15 Ru J, Li P, Wang J, et al. TCMSP: a database of systems pharmacology for drug discovery from herbal medicines. *J Cheminform*. 2014;6:13. https://doi.org/10.1186/1758-2946-6-13.
16 Lin X, Guo X, Qu L, et al. Preventive effect of Atractylodis Rhizoma extract on DSS-induced acute ulcerative colitis through the regulation of the MAPK/NF-κB signals *in vivo* and *in vitro*. *J Ethnopharmacol*. 2022;292:115211. https://doi.org/10.1016/j.jep.2022.115211.
17 Deng M, Chen H, Long J, et al. Atractylenolides (I, II, and III): a review of their pharmacology and pharmacokinetics. *Arch Pharm Res*. 2021;44(7):633-654. https://doi.org/10.1007/s12272-021-01342-6.
18 Pronk S, Páll S, Schulz R, et al. GROMACS 4.5: a high-throughput and highly parallel open source molecular simulation toolkit. Bioinformatics. 2013;29(7):845-854. https://doi.org/10.1093/bioinformatics/btt055.
19 Van Der Spoel D, Lindahl E, et al. GROMACS: fast, flexible, and free. *J Comput Chem*. 2005;26(16):1701-1718. https://doi.org/10.1002/jcc.20291.
20 Hu J, Huang H, Che Y, et al. Qingchang Huashi Formula attenuates DSS-induced colitis in mice by restoring gut microbiota-metabolism homeostasis and goblet cell function. *J Ethnopharmacol*. 2021;266:113394. https://doi.org/10.1016/j.jep.2020.113394.
21 Dai Y, Lu Q, Li P, et al. Xianglian Pill attenuates ulcerative colitis through TLR4/MyD88/NF-κB signaling pathway. *J Ethnopharmacol*. 2023;300:115690. https://doi.org/10.1016/j.jep.2022.115690.
22 Yu H, Wang C, Wu J, et al. Study on the anti-ulcerative colitis effect of pseudoginsenoside RT4 based on gut microbiota, pharmacokinetics, and tissue distribution. *Int J Mol Sci*. 2024;25(2):835. https://doi.org/10.3390/ijms25020835.
23 An J, Liu Y, Wang Y, et al. The role of intestinal mucosal barrier in autoimmune disease: a potential target. *Front Immunol*. 2022;13:871713. https://doi.org/10.3389/fimmu.2022.871713.
24 Odenwald MA, Turner JR. The intestinal epithelial barrier: a therapeutic target. *Nat Rev Gastroenterol Hepatol*. 2017;14(1):9-21. https://doi.org/10.1038/nrgastro.2016.169.
25 Allaire JM, Crowley SM, Law HT, et al. The intestinal epithelium: central coordinator of mucosal immunity. *Trends Immunol*. 2018;39(9):677-696. https://doi.org/10.1016/j.it.2018.04.002.
26 Du WW, Zhou C, Yang H, et al. Aggravated ulcerative colitis *via* circNlgn-mediated suppression of nuclear actin polymerization. *Research*. 2024;7:0441. https://doi.org/10.34133/research.0441. eCollection 2024.
27 Peng J, Li H, Olaolu OA, et al. Natural products: a dependable source of therapeutic alternatives for inflammatory bowel disease through regulation of tight junctions. *Molecules*. 2023;28(17):6293. https://doi.org/10.3390/molecules28176293.
28 Liang J, Dai W, Liu C, et al. Gingerenone A attenuates ulcerative colitis *via* targeting IL-17RA to inhibit inflammation and restore intestinal barrier function. *Adv Sci (Weinh)*. 2024;11(28):e2400206. https://doi.org/10.1002/advs.202400206.
29 Zhang R, Wang Z, Yu Q, et al. Atractylenolide II reverses the influence of lncRNA XIST/miR-30a-5p/ROR1 axis on chemo-resistance of colorectal cancer cells. *J Cell Mol Med*. 2019;23(5):3151-3165. https://doi.org/10.1111/jcmm.14148.
30 Han J, Li W, Shi G, et al. Atractylenolide III improves mitochondrial function and protects against ulcerative colitis by activating AMPK/SIRT1/PGC-1α. *Mediators Inflamm*. 2022;2022:9129984. https://doi.org/10.1155/2022/9129984.
31 Xu L, Zhou Y, Xu J, et al. Anti-inflammatory, antioxidant and anti-virulence roles of atractylodin in attenuating *Listeria monocytogenes* infection. *Front Immunol*. 2022;13:977051. https://doi.org/10.3389/fimmu.2022.977051.
32 Heo G, Kim Y, Kim EL, et al. Atractylodin ameliorates colitis *via* PPARα agonism. *Int J Mol Sci*. 2023;24(1):802. https://doi.org/10.3390/ijms24010802.
33 Yang M, Zhang Q, Taha R, et al. Polysaccharide from *Atractylodes macrocephala* Koidz. ameliorates DSS-induced colitis in mice by regulating the Th17/Treg cell balance. *Front Immunol*. 2022;13:1021695. https://doi.org/10.3389/fimmu.2022.1021695.
34 Kai L, Zong X, Jiang Q, et al. Protective effects of polysaccharides from *Atractylodes macrocephalae* Koidz. against dextran sulfate sodium induced intestinal mucosal injury on mice. *Int J Biol Macromol*. 2022;195:142-151. https://doi.org/10.1016/j.ijbiomac.2021.12.042.
35 Agarwal H, Tinsley B, Sarecha AK, et al. Rap1 in the context of PCSK9, atherosclerosis, and diabetes. *Curr Atheroscler Rep*. 2023;25(12):931-937. https://doi.org/10.1007/s11883-023-01162-7.
36 Khan A, Ni W, Baltazar T, et al. ArhGEF12 activates Rap1A and not RhoA in human dermal microvascular endothelial cells to reduce tumor necrosis factor-induced leak. *FASEB J*. 2022;36(4):e22254. https://doi.org/10.1096/fj.202101873RR.
37 Gündüz D, Troidl C, Tanislav C, et al. Role of PI3K/Akt and MEK/ERK signalling in cAMP/Epac-mediated endothelial barrier stabilisation. *Front Physiol*. 2019;10:1387. https://doi.org/10.3389/fphys.2019.01387.
38 Jiang W, Han YP, Hu M, et al. A study on regulatory mechanism of miR-223 in ulcerative colitis through PI3K/Akt-mTOR signaling pathway. *Eur Rev Med Pharmacol Sci*. 2019;23(11):4865-4872. https://doi.org/10.26355/eurrev_201906_18074.
39 Yan S, Hui Y, Li J, et al. Glutamine relieves oxidative stress through PI3K/Akt signaling pathway in DSS-induced ulcerative colitis mice. *Iran J Basic Med Sci*. 2020;23(9):1124-1129. https://doi.org/10.22038/ijbms.2020.39815.9436.